Journal of Alloys and Compounds 502 (2010) 423–428

Contents lists available at ScienceDirect

Journal of Alloys and Compounds

journal homepage: www.elsevier.com/locate/jallcom

Luminescent properties of the $Sr_{2.97-x}Ba_xMgSi_2O_8:Eu^{2+}{}_{0.01}$, $Dy^{3+}{}_{0.02}$ with different Sr/Ba ratio

Chujun Fu, Yihua Hu*, Yinhai Wang, Haoyi Wu, Xiaojuan Wang

School of Physics and Optoelectronic Engineering, Guangdong University of Technology, Weihuan Xi Road No. 100, Guangzhou, Guangdong 510006, PR China

ARTICLE INFO

Article history:
Received 17 January 2010
Received in revised form 16 April 2010
Accepted 25 April 2010
Available online 4 May 2010

Keywords:
Phosphor
X-ray diffraction
Emission spectrum
Afterglow duration
Thermoluminescence

ABSTRACT

The long afterglow phosphor materials $Sr_{2.97-x}Ba_xMgSi_2O_8:Eu_{0.01}{}^{2+}$, $Dy_{0.02}{}^{3+}$ ($x = 0$, 0.5, 1, 1.5, 2) were prepared by the high temperature solid-state reaction method. The crystal phases of these phosphors were examined using X-ray powder diffraction. Slight shifts of the peaks in the structure, which indicate a small change of the interplanar crystal spacing, were observed for each different x's. As a result of decreasing Sr/Ba ratio, the interplanar spacing becomes widened. The emission peaks of the phosphors indicated on the emission spectra range from 434 to 464 nm under the ultraviolet excitation. By gradually increasing the value of x, the blue shift occurs when $x \leq 1.5$ while the slight red shift occurs when $x > 1.5$. It is probably due to the interfering effect of 5d energy level of Eu^{2+} and the strength of the crystal field which is subjected to the repulsion between the 5d electrons and electron of the ligand and the attraction that exists between Eu^{2+} and the ligand. The thermoluminescence curves depict the depth of the trap, where the Dy^{3+} ion generates, and this leads directly to the long afterglow of the phosphors. As the proportion of Ba in the composition increases, the attenuation time of the long-lasting phosphors shortens. The result of the experiment proves that the luminescent properties of the phosphors can be adjusted with different Sr/Ba ratio.

1. Introduction

Long afterglow phosphor is a special type of luminescent materials that store energy under proper excitation and after the excitation source is switched off, releases the conserved energy by means of visible light, observable in darken surroundings for several hours. The material mentioned above has merited much attention in recent years, for its extensive applications in daily life, such as emergency signing, exterior decoration, luminescent light source, etc. The sulfide and the aluminate-based materials have been widely researched [1–3]. Compared with the sulfide and the aluminate, the silicate-based phosphors have many advantages, such as water resistance and color varieties. In addition, these phosphors are characterized by their physical and chemical stability, availability and relative low cost [4,5]. As a typical of long afterglow material, the alkaline earth silicate is known for the presence of rare earth ion doping in its crystal structure. Several types of silicate-based phosphors have been found and studied, including $Sr_2MgSi_2O_7:Eu^{2+}$, Dy^{3+} [6–9], which have researched the emission and afterglow properties of $Sr_2MgSi_2O_7:Eu^{2+}$, Dy^{3+}, and $Sr_2MgSi_2O_7:Eu^{2+}$ by Dy^{3+}, Nd^{3+} co-doping [10], which has reported the influence on afterglow properties of the phosphors by changing the doped ratio of rare earth ions. Wu et al. [11] have also investigated the controllable optical properties of the $Sr_{1.97-x}Ca_xMgSi_2O_7:Eu^{2+}$, Dy^{3+} by adjusting the ratio of Sr/Ca.

It is generally believed that the phosphorescence of Eu^{2+} ions, in the similar host structure of $R_3MgSi_2O_8$ (R = Ca, Sr, Ba), is caused by the transition between the ground ($^8S_{7/2}(4f^7)$) and the excited ($4f^65d^1$) energy state of Eu^{2+} ions. As the shielding effect of the outer shells, the 4f electrons of Eu^{2+} ions hold relatively unaffected to the variation of the crystal field, however, the 5d electrons split easily according to crystal field changes. The field strength of the Eu^{2+} surroundings determines the peak positions on the emission spectra. Consequently, Eu^{2+} ions can emit visible light with varied colors in the presence of crystal fields of different types [12].

In previous studies, Barry [13] reported that the incorporation of divalent Eu in the compounds $Ba_3MgSi_2O_8$, $Sr_3MgSi_2O_8$, and $Ca_3MgSi_2O_8$ produces phosphors of high luminescence yield. As the alkaline earth ion (Ca, Ba, Sr) radius increase, the emission wavelength becomes shorter. Lin et al. [14] tested a series of Eu and Dy co-doped $R_3MgSi_2O_8$ (R = Ca, Sr, Ba) phosphors, and found that the main emission peaks at 471, 458 and 439 nm, respectively. However, the details of the effect resulting from varying the ratio of Sr/Ba on the luminescent properties phosphors have not been studied. In order to study the influence of the crystal lattice for the different ratio of Sr/Ba phosphors, the $Sr_{2.97-x}Ba_xMgSi_2O_8:Eu^{2+}{}_{0.01}$, $Dy^{3+}{}_{0.02}$

* Corresponding author. Tel.: +86 20 39322262; fax: +86 20 39322265.
E-mail address: huyh@gdut.edu.cn (Y. Hu).

0925-8388/$ – see front matter © 2010 Elsevier B.V. All rights reserved.
doi:10.1016/j.jallcom.2010.04.188

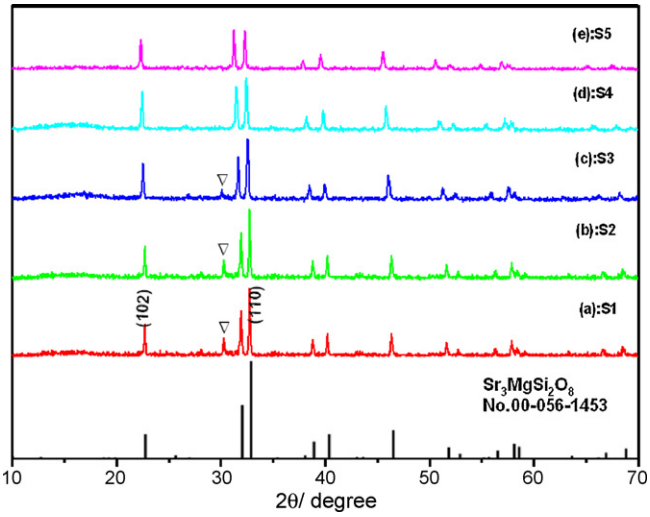

Fig. 1. XRD patterns of the phosphors (S1: Sr/Ba ratio = 2.97:0, S2: Sr/Ba ratio = 2.47:0.5, S3: Sr/Ba ratio = 1.97:1, S4: Sr/Ba ratio = 1.47:1.5, S5: Sr/Ba ratio = 0.97:2).

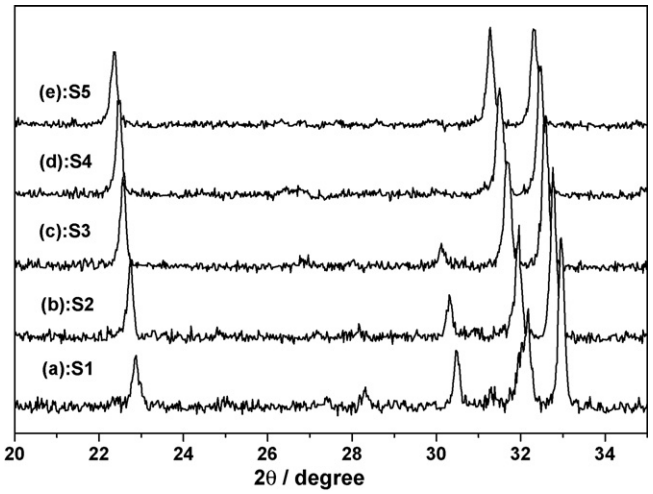

Fig. 2. XRD patterns from 20° to 35° (S1: Sr/Ba ratio = 2.97:0, S2: Sr/Ba ratio = 2.47:0.5, S3: Sr/Ba ratio = 1.97:1, S4: Sr/Ba ratio = 1.47:1.5, S5: Sr/Ba ratio = 0.97:2).

($x = 0, 0.5, 1, 1.5, 2$) are prepared, and their luminescent properties and mechanism are studied in detail.

2. Experimental details

2.1. Synthesis

The compounds $Sr_{2.97-x}Ba_xMgSi_2O_8:Eu_{0.01}{}^{2+}$, $Dy_{0.02}{}^{3+}$ ($x = 0, 0.5, 1, 1.5, 2$) were prepared by the high temperature solid-state reaction method. Analytical purity of $SrCO_3$, $BaCO_3$, SiO_2, MgO, Eu_2O_3, Dy_2O_3 were acted as raw materials. 10 M% H_3BO_3 was added as flux. Composition for each powder was weighed in appropriate stoichiometric ration and mixed thoroughly by 2 h milling in agate mortar. Then, in the high temperature tube furnace, well-mixed powders were sintered at 1300 °C for 3 h with a weak reductive atmosphere of flowing 5%H_2–95%N_2 ensuring complete reduction of Eu^{3+} to Eu^{2+}. The samples obtained are $Sr_{2.97-x}Ba_xMgSi_2O_8:Eu_{0.01}{}^{2+}$, $Dy_{0.02}{}^{3+}$ (where $x = 0, 0.5, 1, 1.5, 2$ and references S1–S5, respectively).

2.2. Characterization

The phase and lattice structure of the synthesized compositions were investigated by X-ray powder diffraction (XRD) using diffractometer with Cu Kα irradiation (λ = 1.5406 Å) at 36 kV tube voltage and 20 mA tube current. The emission spectra can reveal the luminescence property of the materials by a Hitachi F-7000 fluorescence spectrophotometer. Thermoluminescence (TL) glow curves were measured with a Beijing FJ427A1 thermoluminescent dosimeter. The heating rate was 1 K s^{-1} for each sample. All samples were excited upon 254 nm UV for 1 min and the TL testing was carried out 15 min after removing the excitation source. The attenuation curves for the samples were detected by a GFZF-2A single-photon counter system. All the experiments described above were carried out at room temperature.

3. Result and discussion

3.1. XRD phase analysis

In order to explore the crystal phase structure, the XRD phase analysis was adopted. The typical XRD patterns of $Sr_{2.97-x}Ba_xMgSi_2O_8:Eu_{0.01}{}^{2+}$, $Dy_{0.02}{}^{3+}$ ($x = 0, 0.5, 1, 1.5, 2$) phosphors are shown in Fig. 1. The patterns were compared with the JCPDS standard values of the possible phases, which are marked with different symbols. The diffraction peaks in Fig. 1(a) show that the composition is likely $Sr_3MgSi_2O_8$ which was then indexed to the hexagonl system according to JCPDS card no. 56-1453. The lattice parameters calculated were as follows, $a = 5.5$ Å and $c = 13.9$ Å. It can be seen that the crystal phases are similar in Fig. 1, from (a) to (e), which demonstrates that the structure of the host crystal lattice suffers minimum transformation even if the lattice site of Sr is substituted with Ba. Fig. 2 clearly shows that the diffraction peaks shift to lower angle with the decrease of Sr/Ba ratio, which is mainly because the radius of Ba^{2+} ion is larger than Sr^{2+} ion. When Ba ion substitutes the lattice site of Sr ion in the host, the increased radius leads to a larger interplanar crystal spacing d. In response to Bragg equation, $2d \sin\theta = \lambda$, where λ is the wavelength of the X-ray and θ is the incident angle, the d of both (1 0 2) and (1 1 0) interplanar crystal spacing was calculated in Table 1.

Another observation yielded from the XRD patterns is that the phase which probably belongs to another compound (signed with the symbol "▽"), barely even varies as the result shown clearly in Fig. 1. The peaks at about 30.4° may be associated with the (2 1 1) crystal plane of the tetragonal $Sr_2MgSi_2O_7$ structure (JCPDS 1-75-1736). With increasingly higher Ba composition, the intensity of the peak attenuates gradually. When $x > 1$, the peak even disappears completely due to a weaker tetragonal structure with the decrease of the Sr^{2+} content. Therefore, the $Sr_2MgSi_2O_7$ structure disappears.

3.2. Emission spectra

The luminescence emission spectra of $Sr_{2.97-x}Ba_xMgSi_2O_8:Eu_{0.01}{}^{2+}$, $Dy_{0.02}{}^{3+}$ ($x = 0, 0.5, 1, 1.5, 2$) phosphors are shown from (a) to (e), respectively, in Fig. 3. In the measurement, a Xe lamp with 360 nm wavelength was utilized as the excitation source. The result reveals that these five phosphors carry broad-band spectra. As seen in Fig. 3, from (a) to (e), the emission bands peak at 463, 451, 439, 433 and 436 nm, corresponding to S1–S5. This trend well corresponds to the previous report of the photoluminescence of $Sr_{2.97-x}Ba_xMgSi_2O_8:Eu^{2+}$ by Barry [13]. The result shows that ion Eu is only luminescent centre in the phosphors while ion Dy does not contribute to luminescence in this work. The photoluminescence intensity for the samples has been also given in the emission spectra. The sequence of the photoluminescence intensity among the samples is S1 < S2 < S3 < S4 < S5. All these emissions ascribe to the transition from the excited state

Table 1
The diffraction peaks location and the interplanar crystal spacing values.

Samples	(1 0 2)		(1 1 0)	
	2θ (°)	d (Å)	2θ (°)	d (Å)
S1	22.871	3.8851	32.965	2.7149
S2	22.764	3.9031	32.772	2.7305
S3	22.566	3.9370	32.580	2.7462
S4	22.472	3.9532	32.464	2.7557
S5	22.350	3.9745	32.319	2.7677

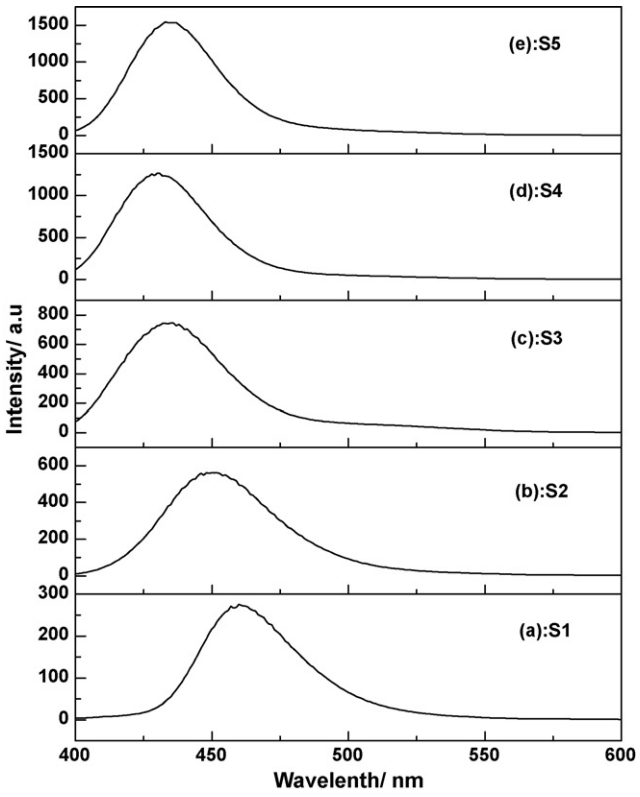

Fig. 3. Emission spectra of the phosphors with 360 nm excitation (S1: Sr/Ba ratio = 2.97:0, S2: Sr/Ba ratio = 2.47:0.5, S3: Sr/Ba ratio = 1.97:1, S4: Sr/Ba ratio = 1.47:1.5, S5: Sr/Ba ratio = 0.97:2).

($4f^6 5d^1$) to the ground state ($4f^7$) configurations of the Eu^{2+} ions [15,16]. No other special emission peaks of Eu^{3+} are observed in the spectra, which proves that Eu^{3+} in the matrix crystals have been reduced to Eu^{2+} completely. The outer 5d orbital of the Eu^{2+} can be influenced by the crystal field in a large extent. Therefore the $4f^6 5d$ energy value can be spread into a continuous band, the emission spectra are shown with a broad band. From Fig. 3, it is also clearly observed that while increasing the value of x, the blue shift is found when $x \leq 1.5$ and also the slight red shift occur when $x > 1.5$. We hypothesize that this trend is probably related to the interelectric attraction and repulsion. Because the radius of Ba^{2+} (0.135 nm) is larger than Sr^{2+} (0.118 nm), the crystal lattice have to expand in order to maintain a stable crystal structure stable when Sr^{2+} ion is replaced by Ba^{2+} ion in the lattice host. This also causes the increase of the crystal plane spacing. It is well known that the 5d layer of the Eu^{2+} ions can separate into two groups according to different energy levels, which can be assigned by t_{2g} (the lowest) and e_g (the highest) [17]. According to Bartwal [18], the actual crystal field symmetry will split these levels further, removing degeneracy completely as the O_h group notation. The electron clouds close to the ligand occupy the higher energy level while the others occupy the lower one. With the increase of the crystal plane spacing, the distance between the Eu^{2+} ions and the ligand become larger. Consequently, the energy of the electrons in the high level will decline as the repulsion between the 5d electrons and electron of the ligand decreases. On the other hand, the average energy of the 5d states holds constant due to the law of conservation of energy, therefore the low energy level will rise, resulting in the blue shift of the emission peak. When the Sr/Ba ratio attains a certain value, the distance between the Eu^{2+} ions and the ligand reaches a balance when the attraction between the Eu^{2+} and the ligand equals the repulsion between the 5d electrons and electron of the ligand. As the Ba composition increases further, the force of attraction will outwin that of the repulsion. As a result, the energy of the electrons in the high level will rise while the low energy level will decline. Consequently, the red shift occurs. The transition of 5d energy states are given in Fig. 4 [18].

3.3. Decay characteristics

The afterglow decay curves of different phosphors with various amounts of Ba were produced by subjecting them to fluorescence lamp for 2 min. The measurement started 30 s later and the curves are shown in Fig. 5. The 2400 s data were also recorded. The result implies that all of the phosphors passed through a rapid decay and then a phase of long-lasting phosphorescence. As shown in Fig. 5, the intensity of S1–S3 at any time is S1 > S2 > S3, and the decay curves of the other two samples almost overlap to the point that they are not distinct from each other on the diagraph. The afterglow duration is evaluated by the curve fitting method. The decay

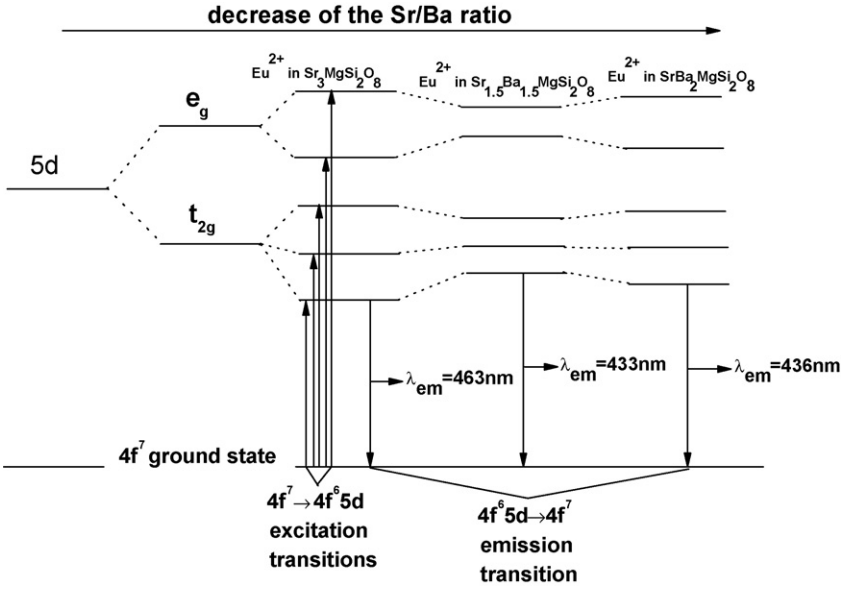

Fig. 4. Schematic diagram of different 5d energy levels of Eu^{2+}.

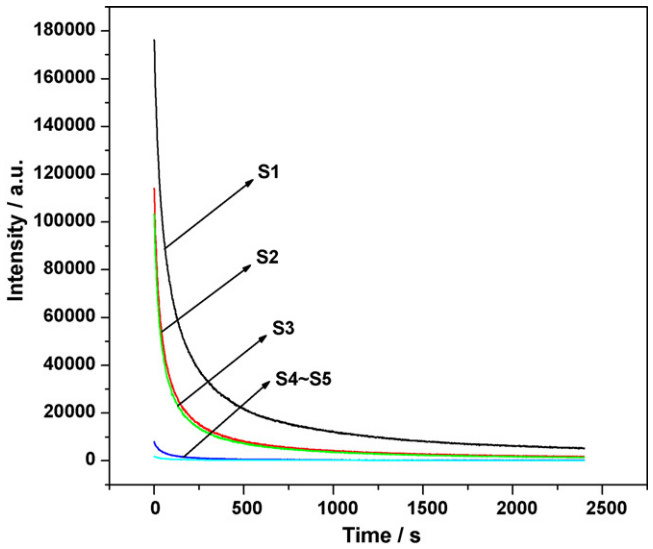

Fig. 5. Decay curves of phosphors with various Sr/Ba ratios (S1: Sr/Ba ratio = 2.97:0, S2: Sr/Ba ratio = 2.47:0.5, S3: Sr/Ba ratio = 1.97:1, S4: Sr/Ba ratio = 1.47:1.5, S5: Sr/Ba ratio = 0.97:2).

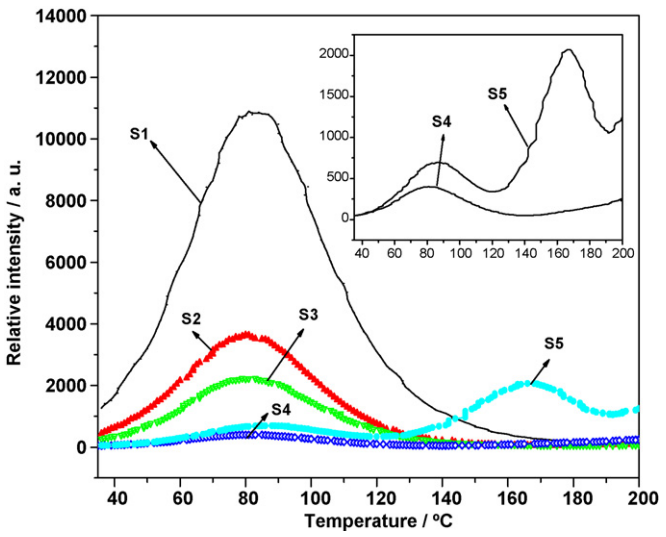

Fig. 6. TL curves of the phosphors (S1: Sr/Ba ratio = 2.97:0, S2: Sr/Ba ratio = 2.47:0.5, S3: Sr/Ba ratio = 1.97:1, S4: Sr/Ba ratio = 1.47:1.5, S5: Sr/Ba ratio = 0.97:2).

curves are fitted to the equation [19]:

$$I = A_1 \exp\left(-\frac{t}{\tau_1}\right) + A_2 \exp\left(-\frac{t}{\tau_2}\right) + A_3 \exp\left(-\frac{t}{\tau_3}\right), \quad (1)$$

where I is the phosphorescence intensity varying with time t; A_1, A_2 and A_3 are three constants, τ_1, τ_2 and τ_3 are attenuation times for the corresponding exponential components. Table 2 shows the attenuation times of different samples. And it can be concluded that when the Ba/Sr ratio increases, the afterglow attenuates faster. In general, S1 shows the best afterglow property among the five samples. When the ratio of Ba/Sr is <1, the afterglow of the phosphors is more obvious, and this is compared to the scenario when the ratio is ≥1, the afterglow of the samples are quite weak.

3.4. Thermoluminescence

In order to conduct a further research on the mechanism of the phosphors, TL glow curves were measured with FJ-427A1 TL meter by heating the irradiated samples from room temperatures to 200 °C. The phosphors were first excited for 1 min using fluorescent lamp. Then the radiation source was removed and the samples were heated at a linear rate of 1 K s^{-1} after 15 min. According to previous studies on the strontium aluminates phosphors (e.g. $SrAl_2O_4$:Eu, Dy [20–22]), it is believed that the co-doped Dy^{3+} works as the hole trap levels and prolongs the afterglow. In earlier reports, it is proposed that the Eu^{2+} ion acts both as an electron trap and as a luminescent center while the R^{3+} (R is rare earth ion) ion serves as a hole trap in the MAl_2O_4:Eu^{2+}, R^{3+} (M is alkaline earth metal) materials [23–26]. This model for long afterglow involves the reduction of Eu^{2+} to Eu^{+} and the oxidation of Dy^{3+} to Dy^{4+} [27–29], which are impossible under near UV or visible excitation due to insufficient energy. The presence of Eu^{+} or Dy^{4+} has not been observed by the X-ray absorption measurements of $SrAl_2O_4$:Eu^{2+}, Dy^{3+} either [30].

Table 2
Fitting parameters for the phosphors samples with various Sr/Ba ratios.

	Samples				
	S1	S2	S3	S4	S5
τ_1 (s)	706.99	549.37	546.82	286.05	215.15
τ_2 (s)	132.90	100.02	98.65	58.19	69.14
τ_3 (s)	28.53	22.11	21.94	14.75	20.65

More recently, Aitasalo et al. [31] have reported that some R^{3+} ions can enhance the persistent luminescence intensity and lengthen the lifetime of afterglow as evidenced by the study of $CaAl_2O_4$:Eu^{2+}, Dy^{3+}, but none of them was found to affect the luminescence wavelength or the shape of the spectrum. And they proposed a new theory on the mechanism of the long afterglow. This mechanism is based on the photoionization of the electrons from Eu^{2+} to the conduction band, and then the electron was trapped to an oxygen vacancy, which is aggregated with a calcium vacancy and an R^{3+} ion. The electrons which migrate from one trap to another and also to the aggregated R^{3+} ion form R^{2+} (or $R^{3+} - e^{-}$). The reverse process of the release of the electron from traps to Eu^{2+} can produce the long afterglow. The mechanism above may be suitable for the silicate-based phosphors in application. That is to say, the long afterglow should be ascribed to the existence of the traps. Moreover, the intensity of luminescence and the afterglow duration depend on the depth of the traps. In a certain concentration of Dy^{3+} traps, the initial intensity will be stronger when the traps are shallow since the trapped carriers will be released more easily. However, if the depth used to trap energy is overly shallow, the phosphors would show a fast decay. If the depth is increased, the energy that releases the carriers from the trap will be greater, and the afterglow will be longer. However, the trap energy level should not be too deep, because the high energy is difficult to obtain at room temperature, and the afterglow will not be obvious. In addition, if the phosphors are heated, the trapped carriers will be released more quickly. Therefore, the higher temperature the carriers need in letting themselves to be released, the deeper trapped energy level is required. As shown in Fig. 6, the TL peaks of S1, S2 and S3 are located at 81, 80 and 83 °C, respectively. And the peak positions are very similar, the order of their intensity is S1 > S2 > S3. The TL peak of S4, which seems similar to the S1–S3, is located at 81 °C, but its intensity is quite weak compared with the other samples. In particular, S5 has two TL peaks, located at 86 and 168 °C, respectively, indicating that S5 have two different kinds of traps. One of the traps is shallow while the other is deep. According to Yonesaki et al. [32], the layer is formed by corner-sharing of MgO_6 octahedra and SiO_4 tetrahedra, Ba^{2+} ion is sited at the center of the interlayer space (A-site) while Sr^{2+} ion is embedded in the layer framework (B-site). Then, the B-site for the glaserite-type structure separates into two sites (B′- and B″-sites) in the merwinite-type structure. This structural transition gives rise to the change in coordination number for alkali-earth-metal ions; the interlayer A-site

Table 3
The calculated trap depths of all the samples.

Samples	T_m (K)	δ (K)	τ (K)	ω (K)	μ_g	E (eV)
S1	354	27	23	50	0.54	0.75
S2	353	25	23	48	0.52	0.73
S3	356	24	25	49	0.48	0.66
S4	354	26	23	49	0.53	0.74
S5[a]	441	24	21	45	0.53	1.30

[a] The low-temperature glow peaks of S5 is too weak to obtain the exact data to calculate the trap depth. The trap depths of S5 in Table 2 only represent the high-temperature glow peak.

cation from 12 in the glaserite-type to 8 in the merwinite-type and the layer-embedded B-site cations from 10 to 8 or 9. From the double traps phenomenon, we could suppose that Dy ions may occupy the two different R (R = Sr, Ba) sites in the lattice host. Hence the coordination environments of Dy^{3+} ions in two structures are quite different, resulting in the two type traps. As seen in Fig. 6, it is obvious that peaks of high-temperature glow predominates, implying that the density of the shallow traps is much smaller than that of the deep traps. That is to say, for S5, the time of afterglow is mainly determined by the trap of the deeper one. The result above conforms well to the decay curves (Fig. 5). Since the depth of the traps of S1, S2 and S3 are suitable to release carriers at room temperature, the afterglow duration are relatively well. In the case of S4, the temperature of the peak is close to the former three samples, which characterizes itself with a small density of shallow traps that exhibit a lower initial intensity and a rapid attenuation curve. As for S5, which find it difficult to release carriers at room temperatures, the afterglows are too weak to be perceivable without the help of instruments. Generally, for phosphors, in order to exhibit long afterglow at room temperatures, it is crucial to have optimized trap level and trap density. The depth of the trap levels could be estimated by TL glow curves (in Fig. 6) fitted to a general order kinetics formula [33]. The TL intensity as a function of temperature, T, is as follows:

$$I(T) = n_0 S \exp\left(\frac{-E}{kT}\right)\left[(b-1)\left(\frac{S}{\beta}\right)\times\int_{T_0}^{T}\exp\left(\frac{-E}{kT}\right)dT+1\right]^{-b/(b-1)}, \quad (2)$$

where n_0 is the concentration of trapped carriers at $t = 0$, and S is the frequency factor, k is the Boltzmann's constant, β is the heating rate, b is the order of kinetics, E is the activation energy (or depth of the trap), which can be calculated from the glow peak parameters by the following equation [7,34,35]:

$$E = \left[2.52 + 10.2(\mu_g - 0.42)\right]\left(\frac{kT_m^2}{\omega}\right) - 2kT_m, \quad (3)$$

where $\omega = \delta + \tau$; δ is the high-temperature half width and τ is the low-temperature half width. The asymmetry parameter $\mu_g = \delta/\omega$. T_m indicates the temperature of the glow peak. The calculated trap depths are listed in Table 3. According to the table, the energy of the shallow traps ranges from 0.66 to 0.75 eV while the deep one is 1.30 eV. These indicate that S1–S3 all have suitable trap depths, in these case, their afterglow duration are greater than other samples. For S5, the energy of the deep traps are much deeper than the former four samples, therefore, they may have difficulty in releasing the carriers at room temperature. As a result, the deep traps may have no contribution to the afterglow. According to Nakazawa et al. [23], the variation of the trap depth with the number of 4f-eletrons is parallel to those of the ionization potential and the system difference of $4f^n$ and $4f^{n-1}5d$. They reported that a smaller ionization potential of rare earth ion leaded to a deeper trap. In this work, when Ba^{2+} ions substitute for Sr^{2+} ions in the host, larger radius of Ba^{2+} leads to larger interplanar crystal spacing. As Dy^{3+} ions occupy the lattice site of R^{2+} (R = Sr, Ca) ions, the repulsion between 4f-electrons and ligand-electrons will decrease. Then 4f-electron clouds will expand since the repulsion decrease. As a result, the ionization potential of Dy^{3+} ions will become smaller. So the trap depth becomes greater as the Ba composition increasing. From the above discussion, the conclusion is that when the ratio of Sr/Ba decreases, the afterglow duration will become shorter.

4. Conclusions

The long afterglow phosphors $Sr_{2.97-x}Ba_xMgSi_2O_8:Eu_{0.01}{}^{2+}$, $Dy_{0.02}{}^{3+}$ ($x = 0, 0.5, 1, 1.5, 2$) were prepared by solid-state reaction method. With the ratio of Ba/Sr increasing, and Ba progressively substituting the lattice of Sr in the host, the interplanar spacing becomes larger while the main structure of the crystal lattice in the host remains relatively unmodified. The emission peak first is towards blue-shift, and then to red-shift right after the value of x is >1.5. This may has an effect on the 5d of the Eu^{2+} and the crystal field strength. The latter being affected by the repulsion between the 5d electrons and electron of the ligand and the attraction that exists between Eu^{2+} and the ligand. The afterglow time becomes shorter when the Ba composition is higher. This is explained by the TL curves which can be used to calculate the depth of the traps. The sample S5 has two TL peaks, low-temperature peak and high-temperature peak, which correspond to shallow trap and deep trap. The samples of S1–S3 composed with suitable shallow traps own longer afterglow duration. And the sample of S5 whose trap level is too deep to release the trapped carriers has shorter afterglow times at room temperature. Thus, we can make the conclusion that adjusting the value of x of the phosphors $Sr_{2.97-x}Ba_xMgSi_2O_8:Eu_{0.01}{}^{2+}$, $Dy_{0.02}{}^{3+}$ ($x = 0, 0.5, 1, 1.5, 2$) can affect the luminescence properties of the materials. In other words, luminescence properties are controllable with different Sr/Ba ratio in the phosphors.

Acknowledgement

This work is supported by the National Natural Science Foundation of China (Nos. 20671022 and 20871033).

References

[1] S.H. Yang, Y.J. Lial, N.J. Cheng, Y.H. Ling, J. Alloys Compd. 489 (2010) 689–693.
[2] C.H. Lu, C.H. Huang, B.M. Cheng, J. Alloys Compd. 473 (2009) 376–381.
[3] J. Zhou, Y.H. Wang, B.T. Liu, Y.H. Lu, J. Alloys Compd. 484 (2009) 439–443.
[4] W. Pan, G. Ning, X. Zhang, J. Wang, Y. Lin, J. Ye, J. Lumin. 128 (2008) 1975–1979.
[5] Y. Xu, D. Chen, Ceram. Int. 34 (2008) 2117–2120.
[6] A.A. Sabbagh Alvani, F. Moztarzadeh, A.A. Sarabi, J. Lumin. 115 (2005) 147–150.
[7] Q. Fei, C. Chang, D. Mao, J. Alloys Compd. 390 (2005) 133–137
[8] B. Liu, C. Shi, M. Yin, L. Dong, Z. Xiao, J. Alloys Compd. 387 (2005) 65–69.
[9] G.B. Zhang, Z.M. Qi, H.J. Zhou, Y.B. Fu, T.L. Huo, X.X. Luo, C.S. Shi, J. Electr. Spectrosc. Relat. Phenom. 144 (2005) 861–863.
[10] H.Y. Wu, Y.H. Hu, Y.H. Wang, B.D. Zeng, Z.F. Mou, J. Alloys Compd. 486 (2009) 549–553.
[11] H.Y. Wu, Y.H. Wang, Y.H. Hu, L.Y. Deng, W. X, J. Phys. D: Appl. Phys. 42 (2009) 125406.
[12] G. Blasse, A. Bril, Philip. Res. Rep. 23 (1968) 201.
[13] T.L. Barry, J. Electrochem. Soc. 115 (1968) 733–738.
[14] Y.H. Lin, Z.L. Tang, Z.T. Zhang, C.W. Nan, J. Alloys Compd. 348 (2003) 76–79.
[15] C. Liu, Y.H. Wang, Y.H. Hu, R. Chen, F. Liao, J. Alloys Compd. 470 (2009) 473–476.
[16] H. Ryu, B.K. Singh, K.S. Bartwal, Physica B 403 (2008) 126–130.
[17] B. Henderson, G.F. Imbush, Optical Spectroscopy of Inorganic Solids, Oxford Science Publications, Oxford, 1989.
[18] K.S. Bartwal, H. Ryu, M.G. Brik, I. Sildos, Physica B 404 (2009) 3440–3444.
[19] T. Katsumata, T. Nabae, K. Sasajima, et al., J. Electrochem. Soc. 144 (1997) L243.
[20] Y. Lin, Z. Zhang, Z. Tang, X. Wang, J. Zhang, Z. Zheng, J. Eur. Ceram. Soc. 21 (2001) 683.
[21] M. Ohta, M. Maruyama, T. Hayakawa, J. Ceram. Soc. Jpn. 108 (2000) 284.
[22] Y. Lin, Z. Zhang, Z. Tang, J. Zhang, Z. Zheng, X. Lu, Mater. Chem. Phys. 70 (2001) 156.
[23] E. Nakazawa, T. Mochida, J. Lumin. 72–74 (1997) 236–237
[24] H. Yamamoto, T. Matsuzawa, J. Lumin. 72–74 (1997) 287–289.
[25] W. Jia, H. Yuan, L. Lu, H. Liu, W.M. Yen, J. Lumin. 76–77 (1998) 424–428.

[26] K. Kato, I. Tsutai, T. Kamimura, F. Kaneko, K. Shinbo, M. Ohta, T. Kawakami, J. Lumin. 82 (1999) 213–220.
[27] M. Kowatari, D. Koyama, Y. Satoh, K. Iinuma, S. Uchida, Nucl. Instrum. Meth. Phys. Res. A 480 (2002) 431–439.
[28] P. Dorenbos, J. Lumin. 104 (2003) 239–260.
[29] P. Dorenbos, J. Lumin. 91 (2000) 155–176.
[30] J. Qiu, M. Kawasaki, K. Tanaka, Y. Shimizugawa, K. Hirao, J. Phys. Chem. Solids 59 (1998) 1521–1525.
[31] T. Aitasalo, J. Hls, H. Jungner, M. Lastusaari, J. Niittykoski, J. Phys. Chem. B 110 (10) (2006) 4589–4598.
[32] Y. Yonesaki, T. Takei, N. Kumada, N. Kinomura, J. Solid State Chem. 182 (2009) 547–554.
[33] T. Katsumata, S. Toyomane, A. Tonegawa, Y. Kanai, U. Kaneyama, J. Cryst. Growth 237–239 (2002) 361–363.
[34] Y. Wang, L. Wang, J. Appl. Phys. 101 (2007) 053108.
[35] Z. Yuan, C. Chang, D. Mao, W. Ying, J. Alloys Compd. 377 (2004) 268–271.